Latin American Journal of Solids and Structures
www.lajss.org

# Analysis of the Dynamic Behavior of a Rotating Composite Hollow Shaft

**Abstract**

In the present paper, a simplified homogenized beam theory is used in the context of a numerical investigation regarding the dynamic behavior of a rotating composite hollow shaft. For this aim, a horizontal flexible composite shaft and a rigid disc form the considered simple supported rotating system. The mathematical model of the rotor is derived from the Lagrange's equation and the Rayleigh-Ritz method, which is obtained from the strain and kinetic energies of the disc and shaft, and the mass unbalance. In this case, a convergence procedure is carried out in terms of the vibration modes to obtain a representative model for the rotor system. Therefore, the proposed analysis is performed in both frequency and time domains, in which the frequency response functions, the unbalance responses, the Campbell diagram, and the orbits are numerically determined. Additionally, the instability threshold of the rotor system is obtained. This study illustrates the convenience of the composite hollow shafts for rotor dynamics applications.

**Keywords**

Rotor dynamics, composite hollow shaft, Rayleigh-Ritz method, numerical investigation.

**Aldemir Ap Cavalini Jr** *
**Thiago A M Guimarães**
**Bruno R M G da Silva**
**Valder Steffen Jr**

LMEst – Structural Mechanics Laboratory, Federal University of Uberlândia, School of Mechanical Engineering, Av. João Naves de Ávila, 2121, Uberlândia, MG, 38408-100, Brazil

* Author email: aacjunior@ufu.br

http://dx.doi.org/10.1590/1679-78253168

Received 15.06.2016
In revised form 04.10.2016
Accepted 24.10.2016
Available online 31.10.2016

## 1 INTRODUCTION

According to Ishida and Yamamoto (2012), research on rotordynamics has over 140 years of history. Its beginning was marked by the work of W.J. Macquorn Rankine (Rankine, 1869), in which the author mistakenly stated that it is impossible for rotating machines to operate above a certain speed. This speed was later called critical speed (Dunkerley, 1894). Simplified basics about

the dynamics of rotating machines was studied by Jeffcott (1919). The work of H.H. Jeffcott led to the development of other essential studies, such as the Campbell diagram, which was first presented by Wilfred Campbell, from General Electric. More effective methods of balancing were proposed and the behavior of rotors supported by hydrodynamic bearings was further investigated, leading to the design of lighter rotating machines operating at higher speeds.

The mathematical representation of the specific physical phenomena that involve rotating machines requires a reliable design tool. In this context, the finite element (FE) method appears as a largely used technique for rotordynamics design. Nelson and MacVaugh (1976) were among the first researchers to include the effects of rotational inertia, gyroscopic moment, and axial force in the FE models. Before the FE method, the so-called transfer matrix method was used to determine the dynamic behavior of rotating machines considering the system as being continuous (Lallement, Lecoanet, and Steffen Jr, 1982). In this context, the modern rotating systems currently employed in various industrial sectors were developed, such as steam turbines, hydro power units, and aircraft engines. These machines present high associated costs and operate under great responsibility and some of them have already composite material components.

Following the growing evolution of the materials used in rotating systems (i.e., materials associated with high performance and low weight), investigations on the dynamic behavior of composite shafts seems to be an important issue. Mazda Motor Corporation adopts hybrid glass and carbon fiber shafts in their cars since 1982. The use of this new technology aims at reducing weight of the rotating system, the cost of maintenance, noise, vibration level, and, at the same time, to increase efficiency as compared with the same components made with traditional metallic materials. Regarding aerospace applications, composite shafts are used in blades and helicopter rotors, and more recently in fixed wing aircraft (as shafts of actuation systems to operate control surfaces). These drive shafts are already found in various aircrafts such as: Airbus A330, A340, A350, A380 and A400M, Bombardier C-Series, Boeing 787, and F-35 JSF (Crompton Technology Group Limited, 2015). Composite materials have interesting properties with respect to rotordynamics (Sino et al., 2008). The following examples can be cited: the high strength to weight ratio, the low resulting weight as compared with metal shafts, and the possibility of optimizing the dynamic behavior of the system aiming at specific characteristics (i.e., changing the number of plies, fiber orientation, material, etc.).

Regarding the research contributions concerning composite shafts, Singh and Gupta (1996) used the equivalent modulus and layer wise beam theories associated with the Rayleigh-Ritz method to determine the mathematical model of a rotor system. The results indicate that the theory based on equivalent modulus beam leads to inaccurate predictions when unsymmetrical stacking sequences with bending stretching couplings are considered. A finite element model associated with a simple disc-shaft system was considered by Chatelet, Lornage, and Jacquet-Richardet (2002), in which the dynamic behavior of the rotating machine was written in terms of its mode shapes. Applications based on a multilayered shell element were carried out to illustrate and validate the proposed model. The dynamic instability of an internally damped rotating composite shaft was evaluated in Sino et al. (2008). The influence of the stacking sequences, fiber orientation, transversal shear effect on natural frequencies, and instability thresholds of the shaft were studied by using the equivalent modulus beam and layer wise beam theories for modeling purposes. In this work, it was shown that

the shaft instability threshold is sensitive to the parameters of the laminate. Particular interest on the damping estimation was presented by Alwan et al. (2010). This work analyzed the dynamic behavior of different materials such as glass/epoxy, carbon/ epoxy, and boron/epoxy considering different rotation speeds. Numerical and experimental analyses were carried out in composite tube-shafts and solid shafts, focusing on the eigenvalues, damping estimation, and unbalance responses of the rotor system. Ren et al. (2014) proposed the mathematical formulation regarding a rotating shaft embedded with shape memory alloy wires. Simulations demonstrated the relationship between the critical speeds of the rotor system and the configuration adopted for the wires. The model took into account the anisotropy of the composite hollow shaft.

In this context, the present paper is dedicated to a numerical investigation regarding the dynamic behavior of a rotating composite shaft. A horizontal flexible composite hollow shaft containing a single rigid disc composes the rotating machine used in this work. The mathematical model of the rotor is derived from the Lagrange's equations and the Rayleigh-Ritz method. In this case, a convergence procedure is carried out in terms of the vibration modes to obtain a representative model for the rotor system. According to Lalanne and Ferraris (1998), the main phenomena that occur in rotordynamics can be evaluated by using this kind of model. Regarding the Lagrange's equations, kinetic energy expressions are used to characterize the disc, the hollow shaft, and mass unbalance. The flexible hollow shaft is described in terms of its strain energy, using the Simplified Homogenized Beam Theory (SHBT) to determine the stiffness (EI). The internal damping of the hollow shaft is incorporated on the Lagrange's equations from its associated virtual work (Sino el al., 2008).

## 2 ROTOR MODEL

Equation (1) gives the differential equation that represents the dynamic behavior of a flexible rotor system operating under steady state condition (Lalanne and Ferraris, 1998).

$$\mathbf{M}\,\ddot{\boldsymbol{\delta}} + \left[\mathbf{D} + \Omega\,\mathbf{D}_g\right]\dot{\boldsymbol{\delta}} + \mathbf{K}\,\boldsymbol{\delta} = \mathbf{W} + \mathbf{F}_u \tag{1}$$

where $\mathbf{M}$ is the mass matrix, $\mathbf{D}$ is the damping matrix (e.g., associated with the bearings), $\mathbf{D}_g$ represents the gyroscope effect, and $\mathbf{K}$ is the stiffness matrix. All these matrices are related to the rotating parts of the system, such as couplings, discs, and shaft. The vector $\boldsymbol{\delta}$ contains the generalized displacements (i.e., the lateral vibrations of the shaft), and $\Omega$ is the shaft rotation speed. $\mathbf{W}$ stands for the weight of the rotating parts and $\mathbf{F}_u$ represents the unbalance forces.

Considering the dissipative effects associated with composite materials (Sino et al., 2006), Equation (1) is them modified as shown by Equation (2).

$$\mathbf{M}\,\ddot{\boldsymbol{\delta}} + \left[\mathbf{D} + \Omega\,\mathbf{D}_g + \mathbf{D}_i\right]\dot{\boldsymbol{\delta}} + \left[\mathbf{K} + \Omega\mathbf{K}_i\right]\boldsymbol{\delta} = \mathbf{W} + \mathbf{F}_u \tag{2}$$

in which $\mathbf{D}_i$ and $\mathbf{K}_i$ are the internal damping and the stiffness matrices, respectively, both associated with the composite material. Note that $\mathbf{K}_i$ is proportional to the rotation speed $\Omega$ imposed to the rotor system. According to (Sino et al., 2006), the anisotropic properties of composite materials and their lightness can be used to optimize composite shafts in order to improve their dynamic behavior. However, compared with the shafts designed from metals, the composite materials present higher associated damping that can induce a destabilizing effect.

As mentioned, the mathematical model of the rotor system used in this work is derived from the Lagrange's equations and the Rayleigh-Ritz method. The rotor is assumed to be simply supported at both ends. Therefore, the displacements along the $x$ and $z$ directions (i.e., $u$ and $w$, respectively), considering any $y$ location along the shaft ($0 \leqslant y \leqslant L$, in which $L$ is the length of the shaft; see Figure 1), are given by Equation (3).

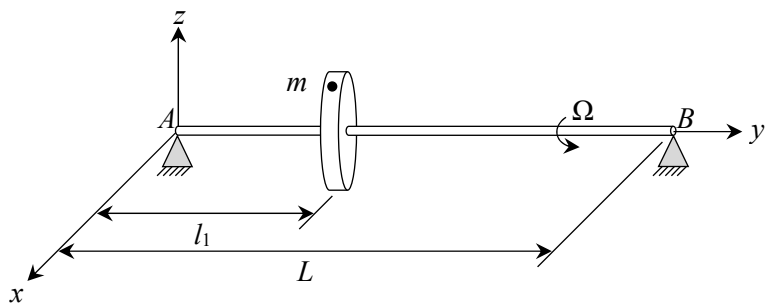


**Figure 1**: Schematic representation of the rotor.

$$\begin{aligned} u(y,t) &= \sum_{r=1}^{n} f_r(y) q_{1r}(t) = f_1(y) q_{11}(t) + f_2(y) q_{12}(t) + \ldots + f_n(y) q_{1n}(t) \\ w(y,t) &= \sum_{r=1}^{n} f_r(y) q_{2r}(t) = f_1(y) q_{21}(t) + f_2(y) q_{22}(t) + \ldots + f_n(y) q_{2n}(t) \end{aligned} \tag{3}$$

in which $q_{1r}(t)$ and $q_{2r}(t)$ are the generalized independent coordinates and $f_r(y)$ are the so-called displacement functions that represent the first $n$ vibration modes associated with each lateral direction of the simple supported rotor system(i.e., assumed-modes method; Lalanne and Ferraris, 1998; Sino et al., 2006; Craig and Kurdila, 2006); $t$ is the simulation time.

Equation (4) presents the considered displacement functions and Figure 2 shows the schematic representation of the first two vibration modes of the simple supported rotor system.

$$f_r\left(y\right) = \sin\frac{r\pi y}{L} \tag{4}$$

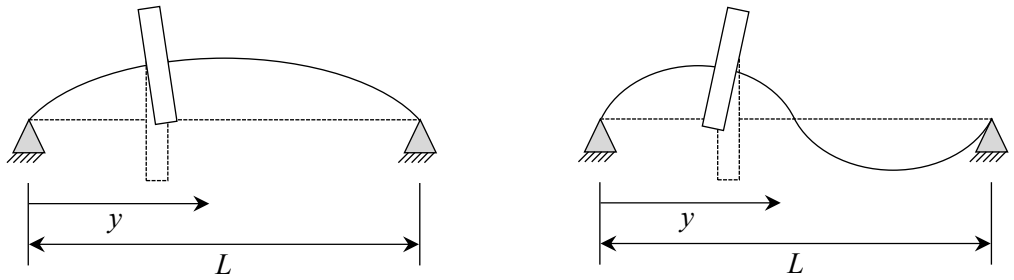


a) $f_1(y) = \sin \pi y/L$. b) $f_2(y) = \sin 2\pi y/L$.

**Figure 2**: Schematic representation of the two first displacement functions.

The angular rotations $\vartheta_u$ and $\vartheta_w$ around the directions $x$ and $z$, respectively (see Figure 1), are small and can be approximated as follows:

$$\theta_u(y,t) = \sum_{r=1}^{n} \frac{df_r(y)}{dy} q_{2r}(t)$$
$$\theta_w(y,t) = -\sum_{r=1}^{n} \frac{df_r(y)}{dy} q_{1r}(t) \tag{5}$$

The geometric properties of the composite hollow shaft are considered constant along they direction (see Figure 1). Therefore, the strain energy $U_s$ of the shaft can be expressed in terms of the homogenized mechanical characteristics as given by Equation (6) (Lalanne and Ferraris, 1998).

$$U_s = \frac{1}{2}\int_0^L \left( EI_x \left( \frac{\partial \theta_u}{\partial y} \right)^2 + EI_z \left( \frac{\partial \theta_w}{\partial y} \right)^2 \right) dy \tag{6}$$

where $EI$ is the homogenized flexural stiffness determined by using the SHBT theory (i.e., symmetric composite shaft leading to $EI = EI_x = EI_z$).

The kinetic energy of the composite shaft $T_s$ is presented by Equation (7) (Lalanne and Ferraris, 1998).

$$T_s = \frac{1}{2}\rho S \int_0^L \left( \dot{u}^2 + \dot{w}^2 \right) dy + \frac{1}{2}\rho I \int_0^L \left( \dot{\theta}_w^2 + \dot{\theta}_u^2 \right) dy + \rho I L \Omega^2 + 2\rho I \int_0^L \dot{\theta}_w \theta_u dy \tag{7}$$

in which $\varrho$ is the volumetric density of the composite material, $S$ is the cross-sectional area of the hollow shaft, and $I$ is the area moment of inertia of the shaft around the directions $x$ and $z$ (see Figure 1).

The kinetic energy of the disc $T_D$ and the mass unbalance $T_u$ are given by (Lalanne and Ferraris, 1998):

$$T_D = \frac{1}{2} M_D \left( \dot{u}^2 + \dot{w}^2 \right) + \frac{1}{2} I_{Dx} \left( \dot{\theta}_u^2 + \dot{\theta}_w^2 \right) + \frac{1}{2} I_{Dy} \left( \Omega^2 + 2\Omega \dot{\theta}_w \theta_u \right)$$
$$T_u = m_u \Omega d \left( \dot{u} \cos \Omega t - \dot{w} \sin \Omega t \right) \tag{8}$$

where $M_D$ is the mass of the disc, $I_{Dx}$ and $I_{Dy}$ are the mass moments of inertia of the disc around the directions $x$ and $y$, respectively, $m_u$ is the unbalanced mass, and d is the distance between the mass $m_u$ to the geometric center of the shaft $C$, as shows the Figure 3.

The differential equations that represent the dynamic behavior of the rotor system are obtained applying first Equation (3) and Equation (5) in the equations of the given strain and kinetic energies. The resulting equations (i.e., the formulated strain and kinetic energies are written by considering the generalized independent coordinates) are applied to the Lagrange's equations (see Equation (9)) (Lalanne and Ferraris, 1998), leading to the mathematical model presented by (see Equation (2)):

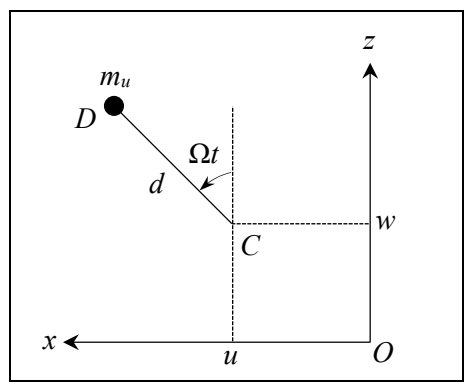


**Figure 3**: Unbalanced mass ($C$ is the center of the deflected hollow shaft).

$$\frac{d}{dt}\left[\frac{\partial(T_s + T_D + T_u)}{\partial \dot{q}_{ir}}\right] - \frac{\partial(T_s + T_D + T_u)}{\partial q_{ir}} + \frac{\partial U_s}{\partial q_{ir}} = Q_{ir}$$
$$\mathbf{M}^q \ddot{\mathbf{q}} + \left[\mathbf{D}^q + \Omega \mathbf{D}_g^q + \mathbf{D}_i^q\right] \dot{\mathbf{q}} + \left[\mathbf{K}^q + \Omega \mathbf{K}_i^q\right] \mathbf{q} = \mathbf{W}^q + \mathbf{F}_u^q \tag{9}$$

where $Q_{ir}$ is the generalized force obtained from the virtual work $\delta W_s$ (see Equation (16); $i = 1, 2$ as showed in Equation (3)), $[.]^q$ stands for matrices and vectors described in the generalized coordinates, and $\mathbf{q}$ is the generalized displacement vector which is given by (see Equation (3)):

$$\mathbf{q} = \left\{ q_{11}(t) \quad q_{21}(t) \quad q_{12}(t) \quad q_{22}(t) \quad \dots \quad q_{1n}(t) \quad q_{2n}(t) \right\}^T \tag{10}$$

In appendix A, the MATLAB® code used to obtain the matrices and vectors of Equation (9) is presented considering the $n$ first vibration modes of the rotor system, for the sake of clarity. The formulation adopted to obtain the matrices $\mathbf{D}_i^q$ and $\mathbf{K}_i^q$ associated with the composite hollow shaft tis presented in the next section. Appendix B presents the numerical evaluation of the Rayleigh-

Ritz model adopted in this work, considering the first natural frequency and the instability threshold of different composite hollow shafts analyzed by Sino et al. (2008).

It is worth mentioning that the Newton-Raphson method in conjunction with the Newmark-type trapezoidal rule integration algorithm was used in this work to determine the vector **q** and, consequently, the lateral displacements of the shaft along the $x$ and $z$ directions by using Equation (3) (i.e., $u$ and $w$, respectively).

## 3 COMPOSITE HOLLOW SHAFT

The composite hollow shaft studied in this work is a *roll wrapped carbon fiber tube* provided by *Easy Composites Ltd*. The shaft is manufactured from a special high-modulus Toray T700 pre-impregnated carbon fiber ply. Figure 4 illustrates the analyzed composite hollow shaft.



**Figure 4**: Composite hollow shaft provided by *Easy Composites Ltd.*

The analyzed composite material has five layers with the following stacking sequence: [0°, 90°, 0°, 90°, 0°]. Table 1 summarizes the physical and geometric properties of the Composite hollow shaft provided by *Easy Composites Ltd* and presented in Figure 4. Table 2 shows the mechanical properties of the analyzed composite material in comparison with two metals, namely the commonly used steel and aluminum materials.

| Inner diameter | Wall thickness | Outer diameter | Stiffness(EI) |
|---|---|---|---|
| 14.0 mm | 1.35 mm | 16.7 mm | 120.0 $Nm^2$ |

**Table 1**: Physical and geometric properties of the composite hollow shaft.

| Property | Composite hollow shaft | Steel | Aluminum |
|---|---|---|---|
| Volumetric density ($kg/m^3$) | 1600.0 | 7800.0 | 2700.0 |
| Young's modulus at 0° (GPa) | 90.0 | 207.0 | 72.0 |
| Young's modulus at 90° (GPa) | 19.0 | 207.0 | 72.0 |
| In-plane shear modulus (GPa) | 4.6 | - | - |
| Major Poisson's ratio | 0.14 | - | - |

**Table 2**: Mechanical properties of the composite hollow shaft in comparison with other materials.

Figure 5 shows a schematic representation regarding the directions of the fibers related to the Cartesian system, which follows the inertial directions defined for the analyzed rotor system (see the inertial directions defined in Figure 1). In this case, 1, 2, and 3 are orthotropic axes associated with the fiber direction, the transversal direction to the fibers in the ply, and the perpendicular direction to the ply, respectively; φ is the angular direction of the fibers (Sino et al., 2008).

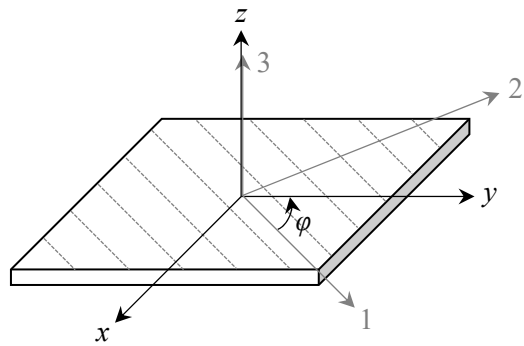


**Figure 5**: Schematic representation regarding the directions of the fibers with respect to the Cartesian system.

The homogenized flexural stiffness *EI* of the composite hollow shaft is determined following the SHBT theory, as is given by Equation (11).

$$EI = \sum_{p=1}^{N} E_y^p I^p$$
$$I^p = \frac{\pi}{4}(R_p^4 - R_{p-1}^4) \tag{11}$$

where $I^p$ represents the inertia moment of area, $R_{p-1}$ is the inner radius, and $R_p$ is the outer radius; all of then associated with the ply $p$. The Young's modulus $E_y^p$ of each ply is obtained by using Equation (12).

$$E_y^p(\varphi) = \frac{1}{\frac{c^4}{E_l} + \frac{s^4}{E_t} + c^2 s^2 \left( \frac{1}{G_{lt}} - 2\frac{\upsilon_{lt}}{E_t} \right)} \tag{12}$$

where $s$ and $c$ stands for $\sin(\varphi)$ and $\cos(\varphi)$, respectively. $E_l$ and $E_t$ are the longitudinal and transversal Young's modulus associated with each ply $p$. The shear modulus is given by $G_{lt}$ and $\upsilon_{lt}$ is the Poisson's ratio.

The parameters given by Table 1 and Table 2 were used to obtain the stiffness *EI* of the hollow shaft by using Equation (11) and Equation (12). The values were compared, resulting a difference of 0.6464% ($EI_{SHBT}$ = 119.2293 Nm$^2$; see the provided stiffness in Table 1). Therefore, the SHBT theory is able to represent the dynamic behavior of the hollow shaft used in this work.

In order to determine the damping and stiffness matrices associated with the composite hollow shaft (i.e., $\mathbf{D}_i{}^q$ and $\mathbf{K}_i{}^q$, respectively; see Equation (9)), the Kelvin-Voigt model (Sino, 2007) was used as shows Equation (13).

$$\sigma = E\varepsilon + \beta E\dot{\varepsilon} \tag{13}$$

where $\sigma$ and $\varepsilon$ are the stress and strain fields, respectively, $E$ is the Young's modulus, $\dot{\varepsilon} = d\varepsilon / dt$, and $\beta$ is a dimensionless parameter. Note that the Kelvin-Voigt model comprises two parts, namely the linear stress-strain relationship given by the Hooke's law and the dissipation properties of the composite material.

The associated virtual work $\delta W_s$ can be written as follows:

$$\delta W_s = \int_0^L \int_S \left(E\varepsilon + \beta E\dot{\varepsilon}\right)\delta\varepsilon dS dy \tag{14}$$

in which the strain field is given by Equation (15).

$$\varepsilon = -z\frac{\partial^2\left(u\cos\Omega t - w\sin\Omega t\right)}{\partial y^2} - x\frac{\partial^2\left(u\sin\Omega t + w\cos\Omega t\right)}{\partial y^2} \tag{15}$$

Applying Equation (15) in Equation (14) and considering $I = \int_s x^2 dS = \int_s z^2 dS$ and $\int_s xz dS = 0$, the virtual work $\delta W_s$ is obtained as show Equation (16).

$$\delta W_s = \beta EI\int_0^L\left(\frac{\partial^2\dot{u}}{\partial y^2}\frac{\partial^2\delta u}{\partial y^2} + \frac{\partial^2\dot{w}}{\partial y^2}\frac{\partial^2\delta w}{\partial y^2} - \Omega\frac{\partial^2 w}{\partial y^2}\frac{\partial^2\delta u}{\partial y^2} + \Omega\frac{\partial^2 u}{\partial y^2}\frac{\partial^2\delta w}{\partial y^2}\right)dy \tag{16}$$

The generalized forces are obtained applying first Equation (3) into Equation (16). The resulting equations are applied on the Lagrange's equations (Lalanne and Ferraris, 1998), leading to the damping and stiffness matrices associated with the composite hollow shaft (Sino, 2007). The homogenized flexural stiffness $EI$ derived from Equation (11) and Equation (12) is also used in Equation (6) to obtain the strain energy $U_s$ of the shaft.

It is worth mentioning that the Rayleigh-Ritz model adopted in the present work follows the formulation presented by Sino (2007) (i.e., SHBT theory associated with the Rayleigh-Ritz model). However, the model was now extended to incorporate other vibration modes in the resulting differential equation of the rotor system (Equation (9)).

## 4 NUMERICAL RESULTS

Figure 1 presents the rotating machine used in the numerical simulations studied in this work. It is composed of a horizontal composite hollow shaft (see Table 1; physic and geometric properties provided by the manufacturer – *Easy Composites Ltd*) with $L = 363.0$ mm length and one rigid disc of steel ($\varrho = 7800.0$ kg/m$^3$) with 150.0 mm diameter and 20.0 mm thickness. The disc is positioned at $y = l_1 = 118.0$ mm (see Figure 1). The rotor is simply supported at points $A$ and $B$ (representation of the bearings). In this work, the dimensionless parameter $\beta$ (Equation (13)) was

considered equal to $1x10^{-5}$. Additionally, the simulations were performed considering the system vibrating around its equilibrium position (i.e., $\mathbf{W}^q = 0$ in Equation (9)).

Figure 6 shows the natural frequencies $\omega_i$ ($i$ = 1, 2, 3, and 4) associated with the first four vibration modes of the rotor system described in this work (i.e., symmetric rotor system; $\omega_1 = \omega_2$ and $\omega_3 = \omega_4$) according to the parameter $n$ used to the expansion of the lateral vibrations $u$, $w$, $\vartheta_u$, and $\vartheta_w$ (see Equation (3) and Equation (5)). In this case, the rotor is at rest. Note that the convergence in terms of the first four natural frequencies of the composite hollow shaft was achieved for $n$ = 35 ($\omega_1 = \omega_2$ = 39.3 Hz and $\omega_3 = \omega_4$ = 184.2 Hz). Therefore, these vibration modes were taken into account in the Rayleigh-Ritz model of the rotor.

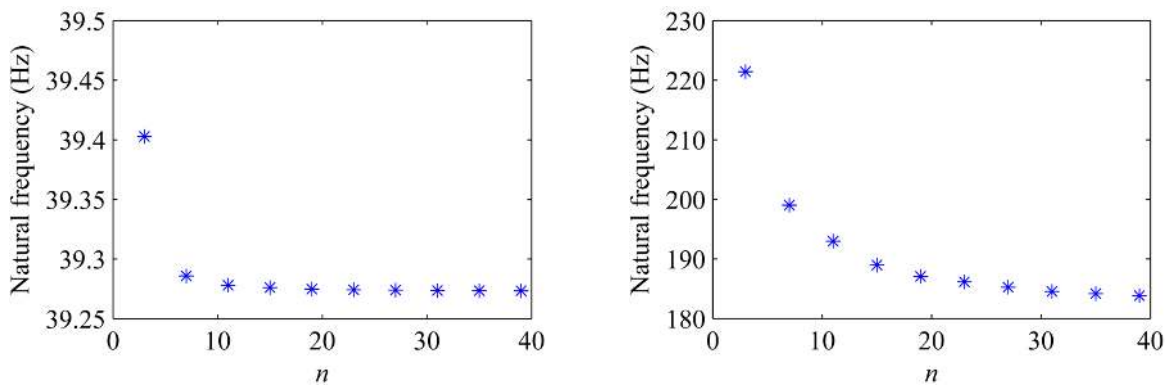


a) $\omega_1 = \omega_2$. b) $\omega_3 = \omega_4$.

**Figure 6**: Natural frequencies associated with the four first vibration modes of the rotor system.

Figure 7 presents the Campbell diagram of the considered rotor system, in which the first forward critical speed in the analyzed frequency band is, approximately, $FW_1$ = 2420 rpm (i.e., close backward and forward whirls; backward critical speeds – $BW_1$ = 2285 rpm and $BW_2$ = 6645 rpm).The instability threshold of the rotor system can be observed in Figure 8, which shows the real part of the eigenvalues associated with the considered vibration modes according to the rotating speed of the composite shaft. Note that the rotor becomes unstable in the vicinity of the first forward critical speed (i.e., approximately 2420 rpm; see Figure 8a). It is worth mentioning that the instability threshold was determined by analyzing the real part of the eigenvalues associated with the four first vibration modes of the system.

Figure 9 presents the unbalance responses of the rotor determined along the $x$ and $z$ directions at the disc position (500 to 3000 rpm in steps of 10 rpm). The instability threshold can be also verified at approximately 2420 rpm (see Figure 8). In this case, an unbalance of $m_u$ = 750 g.mm at $0^o$ was applied to the disc of the rotor.

Figure 10 shows the orbits obtained at the disc position considering the rotor operating under four different rotation speeds: 605 (1/4 of $FW_1$), 806 (1/3 of $FW_1$), 1210 (1/2 of $FW_1$), and 2000 rpm (Figure 10a, 10b, 10c, and 10d, respectively). Note that the vibration amplitude of the rotor system increases with the rotation speed. In this case, only unbalance forces are considered. Additionally, the intrinsic linear characteristic of the adopted Rayleigh-Ritz model can be verified

in the vibration responses associated with the subcritical rotation speeds (1/4, 1/3, and 1/2 of $FW_1$; Figures 10a, 10b, and 10c, respectively). Internal loops should appear in the orbits if a nonlinear behavior had been considered. Figure 10e presents the vibration responses of the rotor operating at 2000 rpm (i.e., determined along the $x$ and $z$ directions).

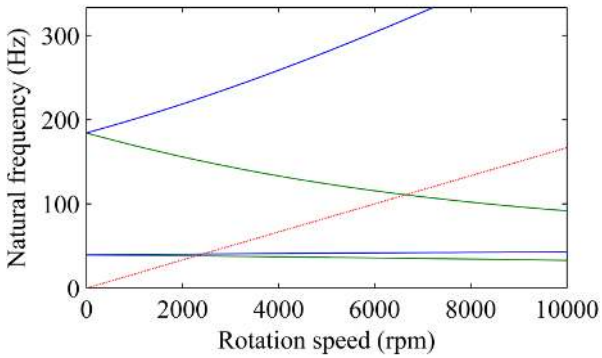


**Figure 7**: Campbell diagram of the considered rotor system (..... $\omega = \Omega$ / 60).

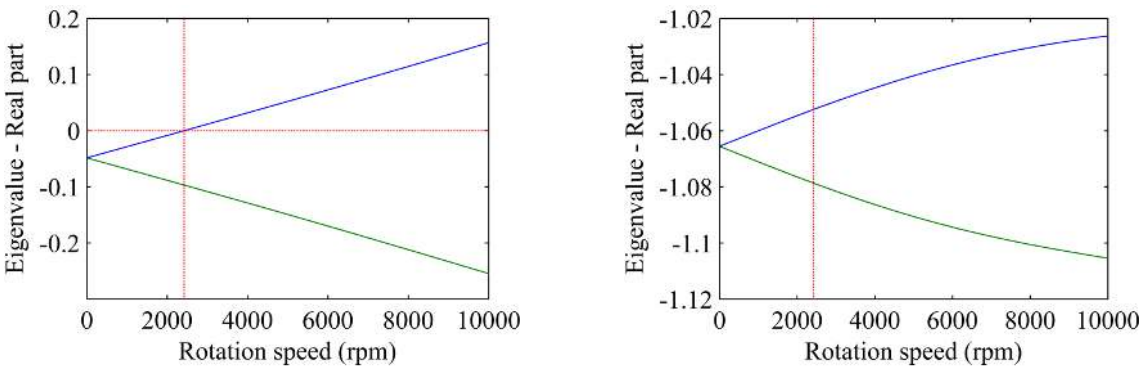


a) First and second vibration modes.

b) Third and fourth vibration modes.

**Figure 8**: Instability threshold of the composite rotor system(.....instability threshold).

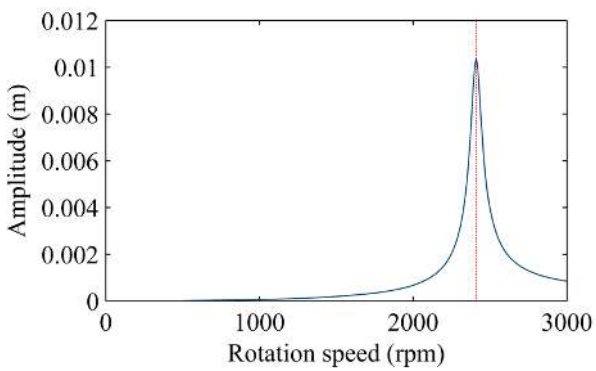


**Figure 9**: Simulated unbalance responses of the rotor and stability limit

(---$x$ direction / ----$z$ direction / ..... instability threshold).

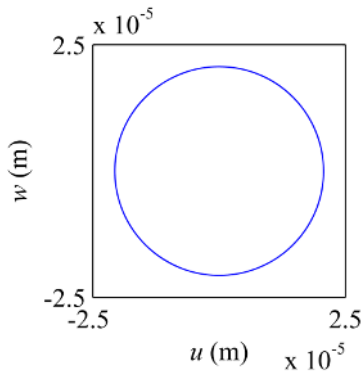


a) Rotation speed = 605 rpm.

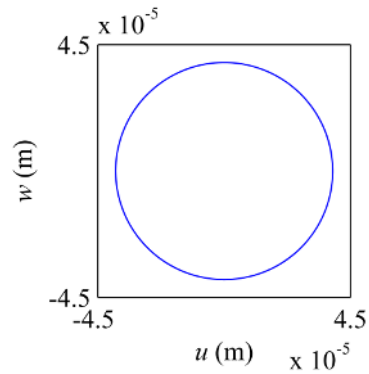


b) Rotation speed = 806 rpm.

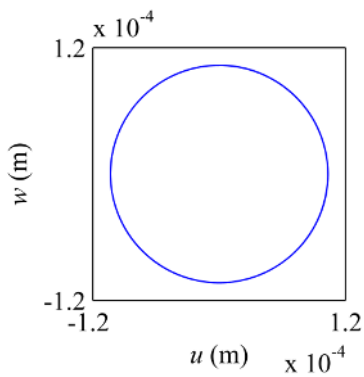


c) Rotation speed = 1210 rpm.

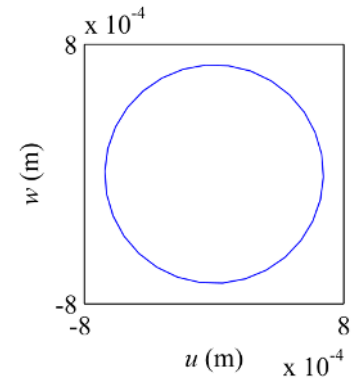


d)Rotation speed = 2000 rpm.

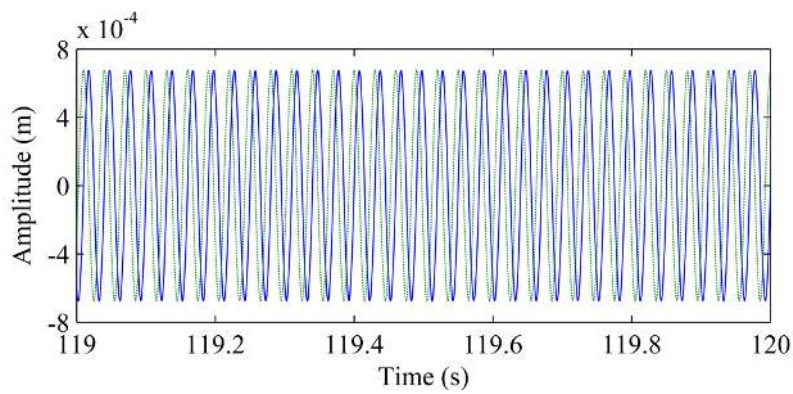


e) Rotation speed = 2000 rpm(----$x$ direction / ····$z$ direction).

**Figure 10**: Vibration responses of the composite hollow shaft operating below the instability threshold.

Figure 11 shows the vibration responses of the rotor operating above the instability threshold, namely 3000 rpm. As expected, the composite rotor shows a stable operating condition considering the rotation speeds lower than the instability threshold (i.e., 605,806, 1210, and 2000 rpm). The unstable condition of the system is demonstrated by the vibration responses obtained for the rotor operating at 3000 rpm. All the simulations were performed from 0 to 120 sec in steps of 0.001 sec.

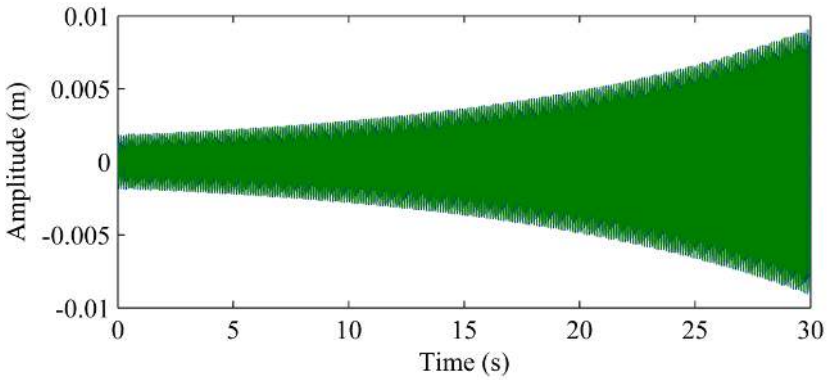


**Figure 11**: Vibration responses of the composite hollow shaft operating at 3000 rpm (----$x$ direction / ----$z$ direction).

## 5 CONCLUSION

In this paper, an investigation regarding the dynamic behavior of a composite hollow shaft was discussed. The rotating machine used in the numerical analyzes is composed by a horizontal composite shaft containing a single rigid disc. The mathematical model of the rotor was derived from the Lagrange's equations and the Rayleigh-Ritz method, which was evaluated considering different composite hollow shafts presented in the literature. The first natural frequency and the instability threshold obtained by the adopted Rayleigh-Ritz model were compared with the results presented by Sino et al. (2008). The natural frequencies obtained from the Rayleigh-Ritz model are similar to those given by Sino et al. (2008). However, significant differences concerning the instability thresholds were verified. In this context, the proposed analyses were performed both in the time and frequency domains, as represented by the orbits, unbalance response, and the Campbell diagram of the composite rotor system. The orbits and unbalance responses were determined from different rotation speeds, in which the dynamic behavior of the considered hollow shaft were analyzed. Further studies will encompass evaluations based on a finite element model for the rotor. An experimental verification is also scheduled.

### Acknowledgements

The authors are thankful to the Brazilian Research Agencies FAPEMIG and CNPq (INCT-EIE) and also to CAPES for the financial support provided to this research effort.

### References

Alwan, V., Gupta, A., Sekhar, A.S., and Velmurugan, R. (2010). Dynamic analysis of shafts of composite materials. Journal of Reinforced Plastics and Composites 29: 3364-3379.

Chatelet, E., Lornage, D., and Jacquet-Richardet, G. (2002). A three dimensional modeling of the dynamic behavior of composite rotors. International Journal of Rotating Machinery 8: 185-192.

Craig, R.R. and Kurdila, A.J. (2006). Fundamentals of structural dynamics. John Wiley & Sons, INC.

Crompton Technology Group Limited. Transmission Shafts. Website: <http://www.ctgltd.com/aerospace-composites >. Accessed on: April 18th 2015.

Dunkerley, S. (1894). On the whirling and vibration of shaft. Philosophical Transactions of the Royal Society of London195: 279-359.

Ishida, Y. and Yamamoto, T. (2012). Linear and nonlinear rotordynamics. Wiley-VCH.

Jeffcott, H.H. (1919). The lateral vibration of loaded shafts in the neighborhood of a whirling speed: the effect of want of balance. Philosophical Magazine A 37: 304-315.

Lalanne, M. and Ferraris, G. (1998). Rotordynamics prediction in engineering. John Wiley & Sons, INC.

Lallement, G., Lecoanet, H., and Steffen Jr, V. (1982). Vibrations de rotors sur paliers à matrice de raideur non symetrique. Machine and Mechanism Theory 17: 47-55.

Nelson, H.D. and Macvaugh, J.M. (1976). The dynamics of rotor bearing systems using finite elements. Journal of Engineering for Industry 98: 593-600.

Rankine, B.J.M. (1869). On the centrifugal force of rotating shafts. The Engineer 1: 1.

Ren, Y., Dai, Q., Na, R., and Zhu, Y. (2014). Modeling and dynamical behavior of rotating composite shafts with SMA wires. Shockand Vibration 2014: 1-16.

Singh, S.P. and Gupta, K. (1996). Composite shaft rotordynamic analysis using a layerwise theory. Journal of Sound and Vibration 2: 179-186.

Sino, R. (2007). Comportement dynamique et stabilité des rotors: application aux rotors composites. l'Institut National des Sciences Appliquées de Lyon, Theses.

Sino, R., Baranger, T.N., Chatelet, E., and Jacquet-Richardet, G. (2008). Dynamic analysis of a rotating composite shaft. Composites Science and Technology 68: 337-345.

Sino, R., Chatelet, E., Baranger T.N., and Jaquet-Richardet G. (2006). Stability analysis of internally damped rotating composite shafts considering transversal shear. Proceedings of ISROMAC - 11, Hawaii USA.

## APPENDIX A

### MATLAB® Code Implemented to Determine the Equation of Motion of the Rotor System

The MATLAB® code used to obtain the matrices and vectors of Equation (9) is presented by Figure A1. In this case, it is considered then first vibration modes of the rotor system.

## APPENDIX B

### Model evaluation

Figure B1a shows the rotating machine (Sino et al., 2008) used to evaluated the Rayleigh-Ritz model adopted in the present work. It is composed of a horizontal composite hollow shaft with $L =$ 1.2 m length, outer radius of 48.0 mm, inner radius of 40.0 mm, and two rigid discs of steel ($\varrho =$ 7800.0 kg/m$^3$) with 150.0 mm diameter and 5.0 mm thickness. The composite hollow shaft is composed by 8 plies (carbon/epoxy material) with the same thickness (i.e., 1.0 mm; see the physic properties in Figure B1b). In Sino et al., (2008), the finite element method was used to represent the dynamic behavior of the rotor system (i.e., 6 finite elements; Timoshenko's beam theory – 2 nodes with 4 degrees of freedom per node) and the composite hollow shaft was supported by flexible bearings (see the stiffness coefficients in Figure B1b). In the present work (Rayleigh-Ritz model), the rotor is simple supported at the ends $A$ and $B$ (representation of the bearings; see Figure B1a). Additionally, $n = 35$ (see Equation (3) and the convergence analysis shown in Figure 6). The dimensionless parameter $\beta$ (Eq. (8)) was considered as equal to $10^{-5}$.

```
% Initialization - n = [~]
syms y L rho S EI I IdxIdy l1 omega Md mu t beta

% Generalized coordinates
k=1;
for i=1:2:2*n-1
    u(i)=sin(k*pi*y/L);
    u(i+1)=0;
    w(i)=0;
    w(i+1)=sin(k*pi*y/L);
    k=k+1;
end

% Mass matrix (Mq)
vud=subs(u,y,l1);                  vwd=subs(w,y,l1);
vdud=subs(diff(u,y),y,l1);         vdwd=subs(diff(w,y),y,l1);
MD=Md*(vud'*vud+vwd'*vwd)+Idx*(vdud'*vdud+vdwd'*vdwd);
M1=rho*S*int(u'*u,y,0,L)+rho*S*int(w'*w,y,0,L);
M2=rho*I*int(diff(u)'*diff(u),y,0,L)+rho*I*int(diff(w)'*diff(w),y,0,L);
Mq=M1+M2+MD;

% Damping and gyroscopic matrix (Cq)
C1=2*rho*I*omega*int(diff(w,y)'*diff(u,y),y,0,L);
C2=-2*rho*I*omega*int(diff(u,y)'*diff(w,y),y,0,L);
C3=-Idy*omega*subs(diff(u,y),y,l1)'*subs(diff(w,y),y,l1);
C4=Idy*omega*subs(diff(w,y),y,l1)'*subs(diff(u,y),y,l1);
Cq=C1+C2+C3+C4;

% Stiffness matrix (Kq)
Kq=int(EI*diff(u,y,2)'*diff(u,y,2),0,L)+int(EI*diff(w,y,2)'*diff(w,y,2),y,0,L);

% Matrices associated with the composite hollow shaft (Ciq and Kiq)
Ciq=beta*EI*(int(diff(u,y,2)'*diff(u,y,2),0,L)+int(diff(w,y,2)'*diff(w,y,2),y,0,L));
Kiq=beta*EI*omega*(int(diff(w,y,2)'*diff(u,y,2),0,L)-int(diff(u,y,2)'*diff(w,y,2),y,0,L));

% Unbalance force (Fuq)
Fuq=mu*omega*omega*(vud*sin(omega*t)+vwd*cos(omega*t));
```

**Figure A1**: MATLAB® code used to obtain the motion equations of the composite rotor system.

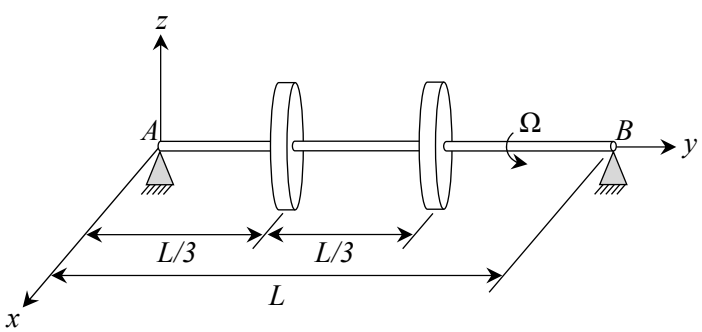


***Composite hollow shaft***

$E_1 = 172.7\ GPa$ $E_2 = 7.2\ GPa$

$G_{12} = 3.76\ GPa$ $\nu_{12} = 0.3$

$\varrho = 1446.2\ kg/m^3$

***Bearings***

$k_{xx} = 10^7 N/m$ $k_{zz} = 10^8 N/m$

a) b)

**Figure B1**: Rotating machine used to validate the Rayleigh-Ritz model adopted in the present work.

Table B1 presents the natural frequencies and instability threshold obtained by Sino et al. (2008) (SHBT theory) and the results determined by the Rayleigh-Ritz model adopted in the present work. In this case, seven different stacking sequences for the composite hollow shaft were taken into account. Note that the natural frequencies determined from the Rayleigh-Ritz model present absolute errors which are smaller than 20% as compared with the ones obtained by Sino et

al. (2008), Regarding the instability thresholds, the maximum difference between the two formulations is smaller than 70%. The presented variations on the instability thresholds can be associated with the formulation used to modeling the internal damping of the composite hollow shaft. In Sino et al. (2008), the internal damping was determined by formulating the damping matrix of each ply of the composite material (the equivalent parameter $\beta$ was used in the present work). However, the Rayleigh-Ritz model is considered as being representative enough for the applications presented.

| Stacking sequence | First natural frequency | | | Instability threshold | | |
|---|---|---|---|---|---|---|
| | Sino (Hz) | RR (Hz)* | Error (%) | Sino (rpm) | RR (rpm)* | Error (%) |
| $[\pm 75]_{8S}$ | 16.88 | 17.14 | 1.54 | 1167 | 1038 | 11.05 |
| $[90_2,45,0]_S$ | 39.87 | 43.86 | 10.01 | 5864 | 2670 | 54.47 |
| [90,0,90,45,90,45,0,90] | 40.08 | 44.05 | 9.91 | 5913 | 2678 | 54.71 |
| $[90,45,0_2]_S$ | 50.71 | 59.36 | 17.05 | 10,981 | 3612 | 67.11 |
| $[0_2,45_2,90_2,0_2]$ | 50.91 | 59.67 | 17.21 | 11,106 | 3630 | 67.31 |
| $[0_2,90,45]_S$ | 50.92 | 59.69 | 17.22 | 11,111 | 3632 | 67.31 |
| [45,0,45,0,90,0,90,0] | 51.36 | 60.37 | 17.54 | 11,395 | 3670 | 67.79 |

* Results determined by the Rayleigh-Ritz model adopted in this work.

**Table B1**: Natural frequencies and instability threshold obtained by Sino et al. (2008) and by the present work.